International Journal of Thermophysics, Vol. 13, No. 1, 1992

Error Analysis of a Ratio Pyrometer by Numerical Simulation[1]

G. R. Gathers[2]

A numerical method has been devised to evaluate measurement errors for a three-channel ratio pyrometer as a function of temperature. The pyrometer is simulated by computer codes, which can be used to explore the behavior of various designs. The influence of the various components in the system can be evaluated. General conclusions can be drawn about what makes a good pyrometer, and an existing pyrometer was evaluated, to predict its behavior as a function of temperature. The results show which combination of two channels gives the best precision.

KEY WORDS: high temperatures; pyrometry; ratio pyrometer; temperature measurement.

1. INTRODUCTION

Various authors have examined the accuracy of multiwavelength pyrometry [1–5]. Gardner [1] examined six-wavelength pyrometry assuming a linear wavelength dependence for the logarithm of the emissivity. He used simulated radiance data altered with uniformly distributed random noise at 0.3% of the radiance value and least-squares fit methods to derive mean temperature and standard deviation. He examined the effect of the number of wavelengths used, spectral range covered, and scattering in the intervening medium and concluded that using extra wavelengths and least-squares methods made little difference in the temperature errors. Simple exact-fit solutions using three wavelengths gave equivalent results. Gardner et al. [2] then built a six-wavelength pyrometer and used non-

[1] Paper presented at the Second Workshop on Subsecond Thermophysics, September 20–21, 1990, Torino, Italy.

[2] Lawrence Livermore National Laboratory, University of California, Livermore, California 94550, U.S.A.

0195-928X/92/0100-0173$06.50/0

linear least-squares methods with a weight function inversely proportional to the wavelength and an emissivity model with linear wavelength dependence. For regions where the emissivity model was a good approximation, the six-wavelength instrument was better than a two-wavelength ratio pyrometer, but for materials where this approximation was poor, the two-wavelength instrument gave superior results. They thus concluded that the accuracy of the measurements was material dependent.

Nordine [3] examined emissivity data for various materials and found that the assumption that emissivity or its logarithm has linear wavelength dependence is often quite poor. He studied emissivity corrections for two, three, and higher wavelengths assuming channels equally spaced in wavelength and found that the emissivity corrections for two-wavelength pyrometers have a greater temperature dependence than those for a single wavelength. As a result, increasing the number of wavelengths used does not increase the accuracy of temperature measurements.

Coates [4] examined the least-squares approach to multiwavelength pyrometry assuming linear wavelength dependence for the emissivity and divided the errors into model and measurement errors. The model errors are those caused by the departure of the actual emissivity from the dependence assumed in the model. As the number of wavelengths used increases, the magnitude of the model errors becomes critically important. The errors also increase as the channel separation decreases, and for practical reasons, increasing the number of wavelengths used is likely to lead to smaller channel separations. The uncertainty in the temperature produced by measurement and systematic errors also increases rapidly with the number of wavelengths used. When extra wavelengths are used giving an overdetermined system and least-squares fitting is used, there is little improvement and the emissivity approximating function must be kept to low order to keep the effects of measurement errors within bounds. Coates concluded that only multiwavelength pyrometers using the exact fit method with three or fewer wavelengths would have acceptable reproducibility and accuracy.

Snopko [5] also divides the error sources into systematic and measurement types. He finds that for the exact fit or determinate calculation, the temperature errors increase rapidly with the number of wavelengths used, but he concludes that for the overdetermined system the measurement errors are decreased.

Various authors [6–10] have used multiwavelength pyrometers. Those considering moderate to high temperatures [1–5, 7–9] use the Wien approximation, while those interested in very high temperatures [6, 10, 11] use the Planck law. Most authors [1–9] assume a linear wavelength dependence for the logarithm of the emissivity. Some of them [1–4] con-

sider higher-order polynomials for the dependence, while others [10, 11] use constant emissivity. The quantity that is minimized when least-squares fitting is used varies considerably.

In the present paper, a computer code is developed for rapid evaluation of a simple two-channel pyrometer assuming constant emissivity. The calculation allows examination of the predicted performance as a function of temperature for any proposed choice of components for the instrument. Measurement errors are determined for the worst case in the ratio for an assumed uncertainty in the detector data signals. The total accuracy, of course, is not known since the actual emissivity dependence on wavelength and temperature is ignored. The systematic errors due to inadequacy of the emissivity model are thus not considered. The method examines only the influence of measurement errors. The technique determines the maximum bounds of the temperature calculation and allows one to determine what makes the best design for this type of pyrometer. Extension of the method to a three-channel pyrometer using an emissivity with linear wavelength dependence and arbitrary temperature dependence is considered in the following paper [12].

2. METHOD

The passband characteristics of the detectors and optical system are assumed to be known. We have

$$R_i(T) = G\varepsilon \int_0^\infty D_i(\lambda)\, B_i(\lambda)\, W(\lambda, T)\, d\lambda \tag{1}$$

as the response of a channel, where $D_i(\lambda)$ describes the detector, $B_i(\lambda)$ describes the combined effect of all optical elements for the channel, and $W(\lambda, T)$ is the spectral density of an ideal blackbody. The emissivity ε is assumed constant and is thus taken outside the integral. G is a normalizing constant, assumed to be the same for all channels. It includes such things as the solid angle attenuation. Tables of the integral as a function of temperature can be calculated for each channel and constitute the description of the pyrometer. We assume three channels for our example.

The ratios R_1/R_2, R_1/R_3, and R_2/R_3 can be calculated as a function of temperature from the integral tables and stored as an additional set of tables. The experimentally observed ratio at a given point in time is used to interpolate in the ratio table for the corresponding channels to determine the temperature.

To test the design, a linear ramp of temperature versus time is assumed and the integral tables are used to calculate the corresponding

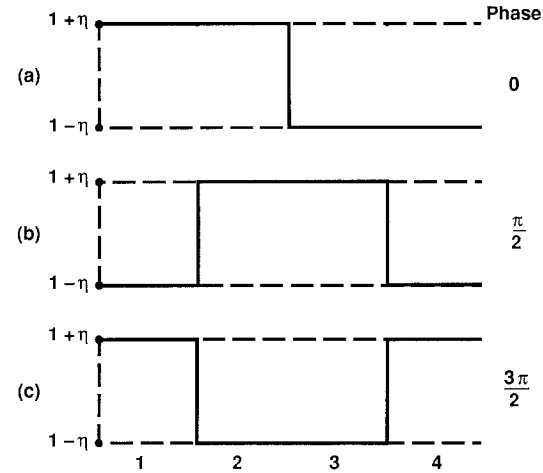

Fig. 1. Square wave modulation used for each channel of the three-channel ratio pyrometer: (a) Ch1; (b) Ch2; (c) Ch3.

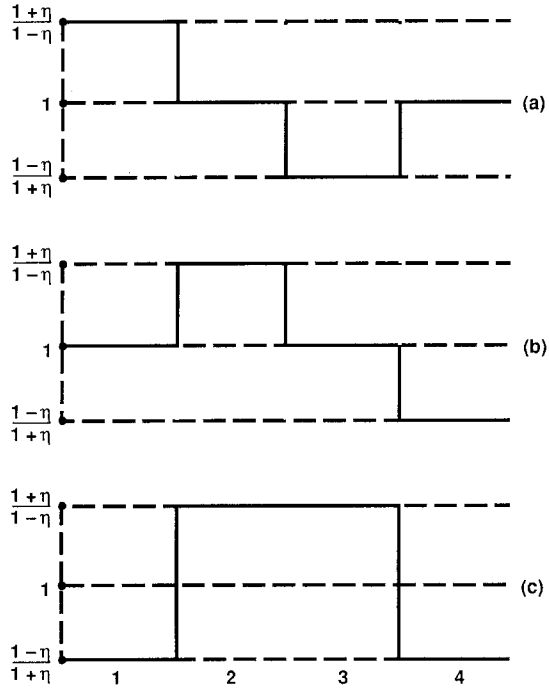

Fig. 2. Effective modulation of the ratio for the three combinations of channels: (a) Ch1/Ch2; (b) Ch1/Ch3; (c) Ch2/Ch3.

response versus time for each channel. Errors are then injected into this artificial data by modulating the calculated responses with square waves of amplitude $1+\eta$, where 100η is the assumed percentage error. The relative phases of the square waves are chosen so that the ratio for each channel combination alternates between the maximum and the minimum (i.e., for the maximum, the ratio is effectively multiplied by $(1+\eta)/(1-\eta)$ and for the minimum it is multiplied by the reciprocal of this).

Figure 1 shows the square wave used for each channel, and Fig. 2 shows the corresponding effect on each ratio. These altered artificial data are then processed by the data reduction code for the pyrometer. Since the relative time of the temperature excursions produced by the modulation is known, the temperature history for each channel combination can be

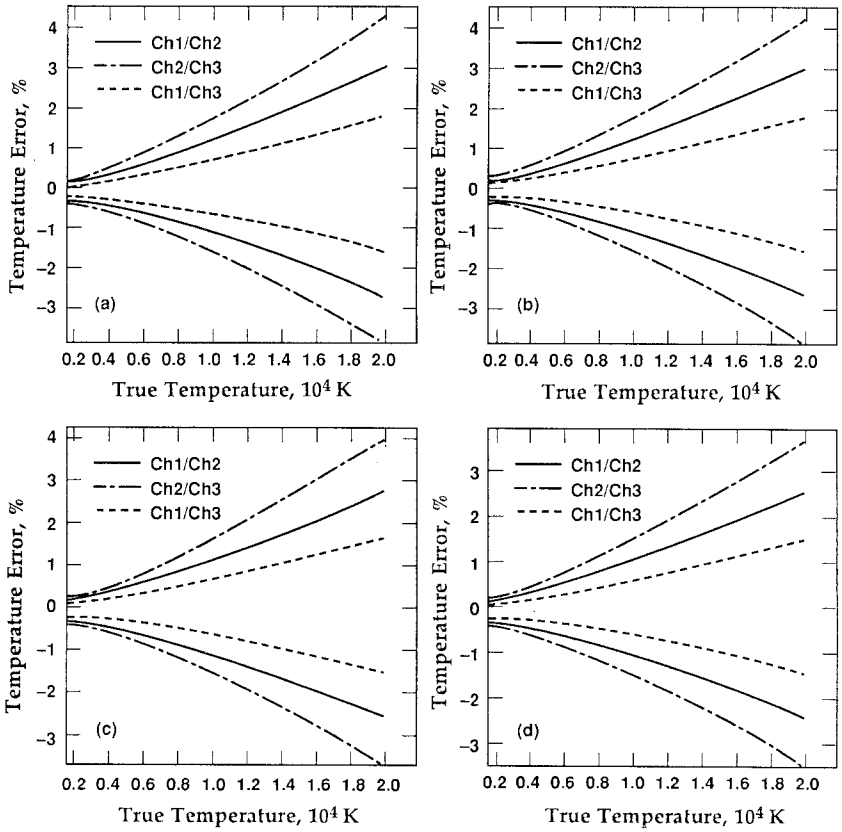

Fig. 3. Dependence of temperature measurement errors on channel bandwidth using 0.2% input data errors and Gaussian channels located at 550, 650, and 750 nm: (a) 20-nm FWHM; (b) 50-nm FWHM; (c) 100-nm FWHM; (d) 150-nm FWHM.

sampled to pick points of maxima and minima. Fitting curves to the points allows calculation of the percentage deviation from the exact result for each channel combination as a function of temperature.

3. RESULTS

Gaussian channel responses were used to explore the influence of bandwidth and channel separation on the precision. In each case, 0.2% input data errors were used. Figure 3 shows the results for channels located at 550, 650, and 750 nm with various bandwidths. It can be seen that channel width is not a sensitive variable. Figure 4 compares results for channels with 50-nm full width at half-maximum (FWHM), located at 550, 650, and 750 nm and at 500, 700, and 900 nm. It can be seen that channel spectral location is important. The best results are obtained by using wide channel separation. It can also be seen that the measurement errors begin to increase rapidly as the temperature increases.

Figure 5 shows the channel locations and widths versus the spectral maximum for a series of temperatures. Gaussian channels with 50-nm FWHM, located at 550, 650, and 750 nm, were used. At high temperatures the channels are located on the red side of the spectral maximum. Figure 6 shows the ratios for this pyrometer as a function of temperature. The increase in measurement errors is due to the saturation in the curves. At high temperatures a small deviation in the ratios corresponds to a large deviation in temperature. The smallest measurement errors are obtained when the channels are all on the blue side of the spectral maximum.

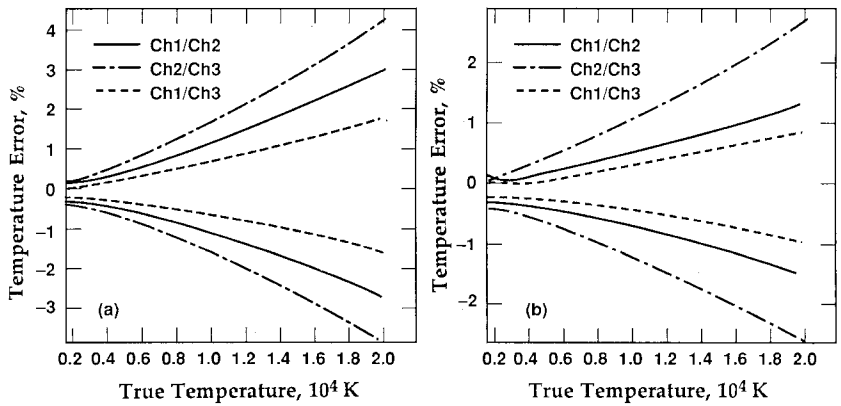

Fig. 4. Dependence of temperature measurement errors on channel spectral location, using 0.2% input data errors and Gaussian channels with FWHM of 50 nm: (a) 550, 650, and 750 nm; (b) 500, 700, and 900 nm.

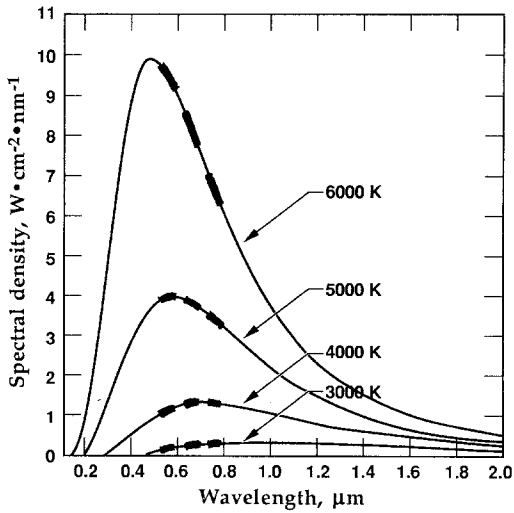

Fig. 5. Channel spectral locations and widths versus the spectral maximum for a series of temperatures. Gaussian channels with 50-nm FWHM, located at 550, 650, and 750 nm, were used. The widths shown correspond to the half-maximum points.

The above results show that for very high temperatures ratio pyrometry is not very practical, because the need to keep channels on the blue side of the spectral maximum forces them to be in the ultraviolet (UV), where suitable detectors and filters are not readily available.

The above method of analysis was used to evaluate an existing pyrometer in the laboratory. Figure 7 shows the construction schematically. It uses beam-splitters, filters, and RCA 8575 and RCA C31000 photo-

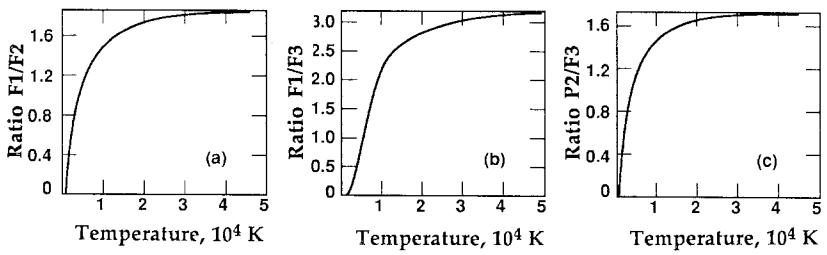

Fig. 6. Channel ratios versus temperature for Gaussian channels located at 550, 650, and 750 nm with 50-nm FWHM.

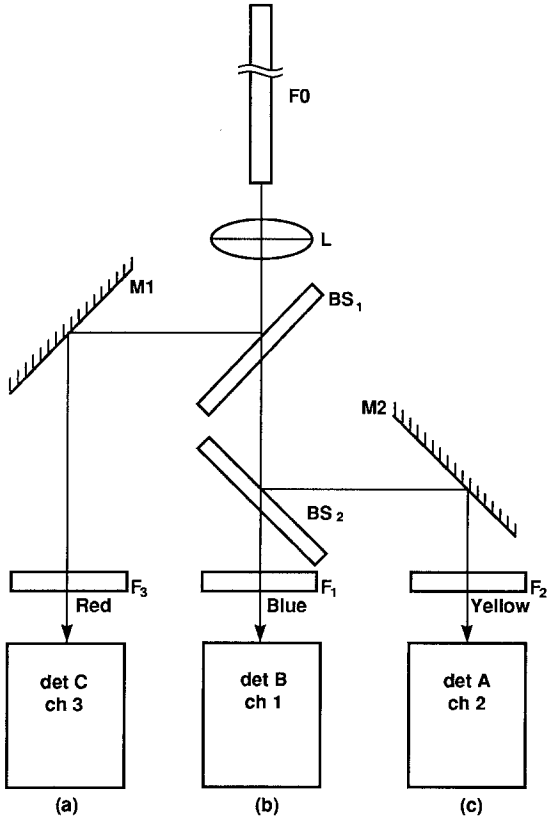

Fig. 7. Example pyrometer using beam-splitters, filters, and photomultipliers. (a) RCA C31000; (b) RCA 8575; (c) RCA 8575. L, lens; M, mirror; BS, beam-splitter; F, filter; FO, fiber-optic light-pipe.

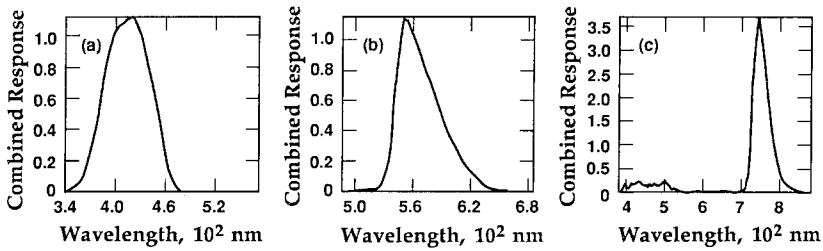

Fig. 8. Spectral response for each channel of the pyrometer shown in Fig. 7 without the fiber-optic light-pipe. (a) Ch1; (b) Ch2; (c) Ch3.

multiplier detectors. The pyrometer was designed for use in hostile environments with explosives, so it is equipped with a fiber-optic light-pipe. The response of the pyrometer itself must be multiplied by the fiber response to calculate the correct integrals. The fiber-optic light-pipe is a length of Ensign Brickford HCS-610-T optical fiber. In use, a portion of the light-pipe is lost on each shot, so that one must recalibrate the light-pipe and generate new blackbody integral tables for the new combination of pyrometer and light-pipe. Figure 8 shows the spectral response of each channel without the light-pipe. A scanning digital monochromator was used to determine directly the combined response of detectors and other optical elements for each channel. This technique was described by Coppa et al. [13], but here the correction for the variation in the monochromator output with wavelength is performed automatically for the instrument used. For one of the channels it may be noted that there is a significant subsidiary response in the UV. Commercial filters often have such a response without it being mentioned by the manufacturer. Since the mirrors and beam-splitters are polarizing elements, one must measure the response for each of two polarizations and take the average when using the pyrometer with unpolarized radiation. Figure 9 shows the spectral response of the 6.5-m long fiber-optic light-pipe.

Figure 10 shows results for the pyrometer with the fiber-optic light-pipe attached. The input data have 0.2% errors. Figure 11 shows the

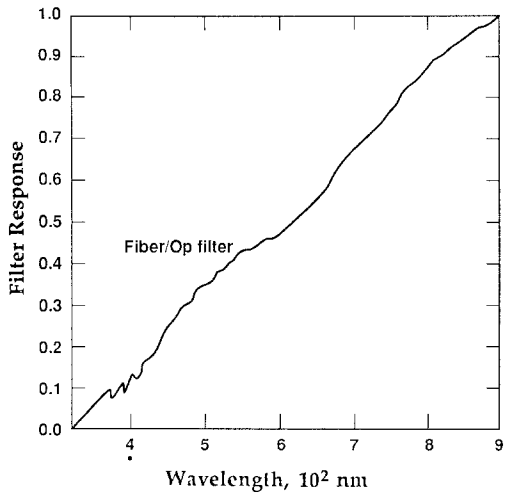

Fig. 9. Spectral response of the 6.5-m length of Ensign Brickford HCS-610-T fiber-optic light-pipe.

results without the fiber-optic light-pipe. It can be seen that for the case of channel 2/channel 3 the light-pipe makes a considerable improvement. This result would not have been intuitively obvious. It may also be seen that for temperatures below 10,000 K the instrument performs quite satisfactorily.

A Monte Carlo analysis was made using the example pyrometer with the fiber-optic light-pipe attached. Simulated data were generated and randomly distributed errors of $\pm 0.2\%$ of the signal level were added to the data. A series of 10 runs was made using a randomly chosen seed for each run. At each time point 10 temperatures were thus calculated for each channel combination and were used to calculate the mean and standard deviation. The resulting curves of standard deviation versus temperature for each channel combination were smoothed by least-squares fitting and

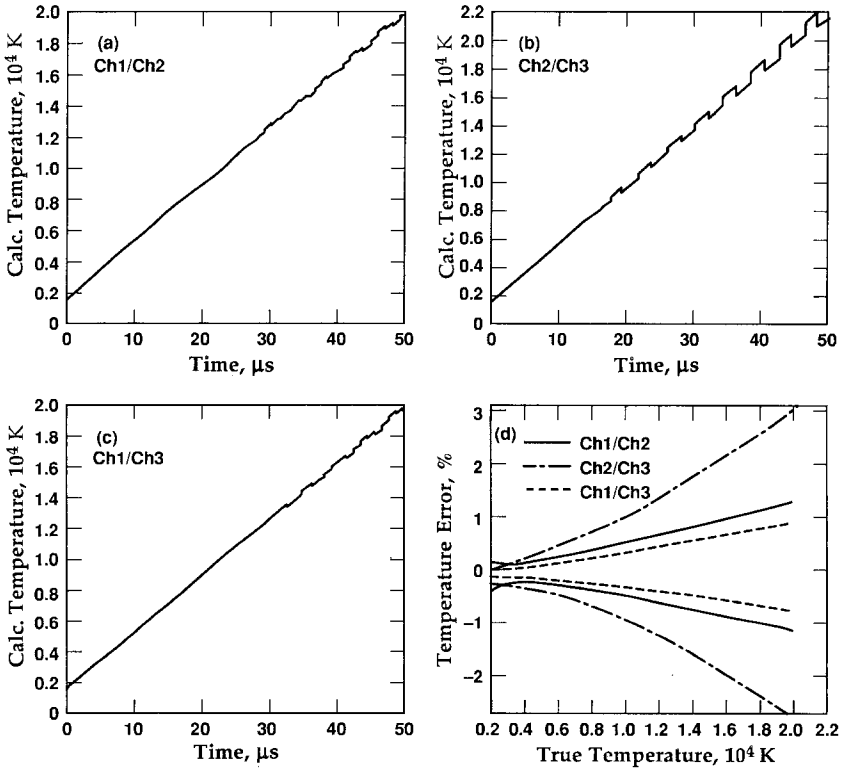

Fig. 10. Temperature measurement errors for the pyrometer in Fig. 7 with the fiber-optic light-pipe attached, using 0.2% input data errors. (a–c) The temperature displacements caused by the modulation; (d) The corresponding percentage errors.

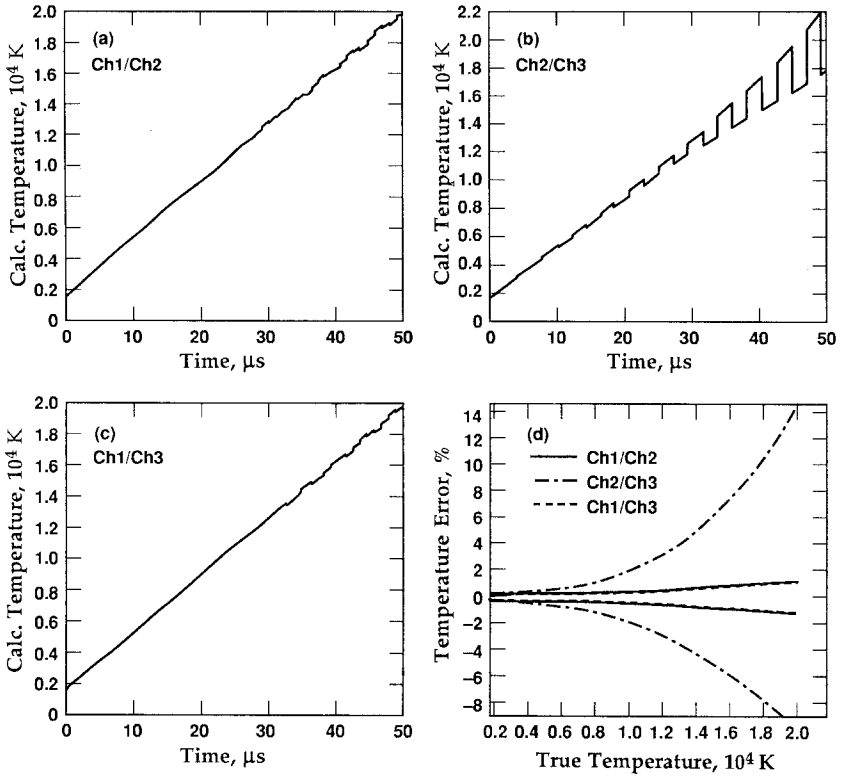

Fig. 11. Temperature measurement errors for the pyrometer in Fig. 7 without the fiber-optic light-pipe, using 0.2% input data errors. (a–c) The temperature displacement caused by the modulation; (d) The corresponding percentage errors.

are shown in Fig. 12. Comparison with Fig. 10 shows that the error curves from the modulation method are approximately proportional to 2.7 standard deviations for all combinations and temperatures. It can thus be seen that the modulation method gives results comparable to the Monte Carlo results for much less computer time.

4. CONCLUSIONS

Computer simulation has shown that the measurement errors for a ratio pyrometer assuming constant emissivity are least when the channels are widely separated in wavelength and located on the blue side of the spectral maximum.

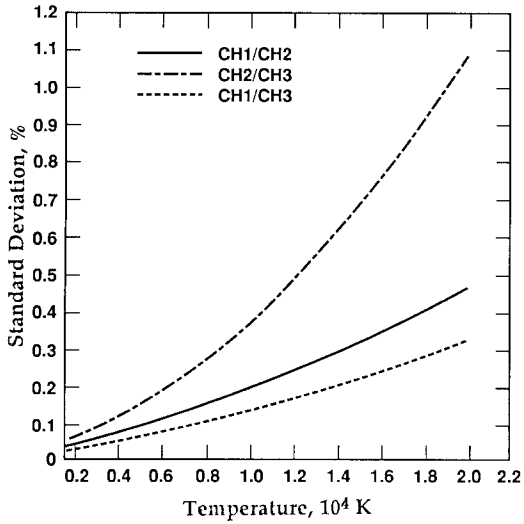

Fig. 12. Standard deviation for the temperature calculated for each channel combination as a function of temperature. The results were derived using Monte Carlo methods, with input data errors uniformly distributed in the range $\pm 0.2\%$.

The bandwidth of the channel response is not critical and may be made relatively wide to give greater sensitivity and hence operation at lower temperatures or be made narrow to avoid possible line radiation which may be present. The spectral response of the entire system including all optical elements must be accounted for in calculating the blackbody integral tables. The analysis allows prediction of the performance of a given design from the optical response of the components. While the analysis here is for ratio pyrometers, it can be readily adapted to brightness pyrometers as well.

ACKNOWLEDGMENT

This work was performed under the auspices of the U.S. Department of Energy by the Lawrence Livermore National Laboratory under Contract W-7405-ENG-48.

REFERENCES

1. J. L. Gardner, *High Temp. High Press.* **12**:699 (1980).
2. J. L. Gardner, T. P. Jones, and M. R. Davies, *High Temp. High Press.* **13**:459 (1981).
3. P. C. Nordine, *High Temp. Sci.* **21**:97 (1986).

4. P. B. Coates, *High Temp. High Press.* **20**:433 (1988).
5. V. N. Snopko, *High Temp.* **25**:724 (1987).
6. G. A. Lyzenga and T. J. Ahrens, *Rev. Sci. Instrum.* **50**:1421 (1979).
7. J. Hiernaut, R. Beukers, W. Heinz, R. Selfslag, M. Hoch, and R. W. Ohse, *High Temp. High Press.* **18**:617 (1986).
8. J. Hiernaut, F. Sakuma, and C. Ronchi, *High Temp. High Press.* **21**:139 (1989).
9. J. L. Babelot and M. Hoch, *High Temp. High Press.* **21**:79 (1989).
10. M. B. Boslough and T. J. Ahrens, *Rev. Sci. Instrum.* **60**:3711 (1989).
11. H. B. Radousky and A. C. Mitchell, *Rev. Sci. Instrum.* **60**:3707 (1989).
12. G. R. Gathers, *Int. J. Thermophys.* **13**:187 (1992).
13. P. Coppa, G. Ruffino, and A. Spena, *High Temp. High Press.* **20**:479 (1988).